A Facile Stratification-Enabled Emergent Hyper-Reflectivity in Cholesteric Liquid Crystals

Qunmei Wei[a], Pengrong Lv[b], Yang Zhang[a,c], Jiwen Zhang[a], Zhuofan Qin[d], Laurens T. de Haan[a,c,*], Jiawen Chen[c], Ding Wang[d], Ben Bin Xu[d], Dirk J. Broer[a,b], Guofu Zhou[a,c,e], Liming Ding[f], Wei Zhao[a,c,*]

[a] *SCNU-TUE Joint Lab of Device Integrated Responsive Materials (DIRM), National Center for International Research on Green Optoelectronics, South China Normal University, No 378, West Waihuan Road, Guangzhou Higher Education Mega Center, 510006, Guangzhou China*

[b] *Stimuli-responsive Functional Materials and Devices, Department of Chemical Engineering and Chemistry, Eindhoven University of Technology, Den Dolech 2, Eindhoven, 5600 MB, The Netherlands*

[c] *Guangdong Provincial Key Laboratory of Optical Information Materials and Technology & Institute of Electronic Paper Displays, South China Academy of Advanced Optoelectronics, South China Normal University, Guangzhou 510006, P. R. China*

[d] *Mechanical and Construction Engineering, Faculty of Engineering and Environment, Northumbria University, Newcastle upon Tyne, NE1 8ST, UK*

[e] *Shenzhen Guohua Optoelectronics Tech. Co. Ltd., Shenzhen 518110, P. R. China*

[f] *Center for Excellence in Nanoscience (CAS), Key Laboratory of Nanosystem and Hierarchical Fabrication (CAS), National Center for Nanoscience and Technology, Beijing 100190, China*

* Corresponding authors.

E-mail address: ldhaan@m.scnu.edu.cn (L.T. de Haan), weizhao@m.scnu.edu.cn (W. Zhao)

Keywords: Photopolymerization-enforced stratification; phase separation; hyper-reflectivity; cholesteric liquid crystals; chiral dopant bundle

ABSTRACT

Cholesteric liquid crystals (CLCs) are chiral photonic materials with selective reflection in terms of wavelength and polarization. Helix engineering is often required in order to produce desired properties for CLC materials to be employed for beam steering, light diffraction, scattering, adaptive or broadband reflection. Here, we demonstrate a novel photopolymerization-enforced stratification (PES)-based strategy to realize helix engineering in a chiral CLC system with initially one handedness of molecular rotation throughout the layer. PES plays a crucial role to drive the chiral dopant bundle consisting of two chiral dopants of opposite handedness to spontaneously phase separate, and create a CLC bilayer structure that reflects left- and right-handed circularly polarized light (CPL). The initially hidden chiral information therefore becomes explicit, and hyper-reflectivity, *i.e.*, reflecting both left- and right-handed CPL, successfully emerges from the designed CLC mixture. The PES mechanism can be applied to structure a wide range of liquid crystal (LC) and polymer materials. Moreover, the engineering strategy enables facile programming of the center wavelength of hyper-reflection, patterning, and incorporating stimuli-responsiveness in the optical device. Hence, the engineered hyper-reflective CLCs offers great promises for future applications, such as digital displays, lasing, optical storage, and smart windows.

1 INTRODUCTION

Cholesteric liquid crystal (CLC) type structures widely exist in nature, *e.g.* the condensed phase of DNA, plant cell walls, arthropod cuticles, human dense bone, and many chiral biomaterials.[1–5] The self-organized helical structure possesses unique optical properties.[6–9] In a conventional CLC, the light is reflected when the wavelength within the medium matches the pitch of cholesteric helical structure.[10–13] The reflectance is limited to 50% for normally incident unpolarized light due to polarization selectivity. The bandwidth, measured as the width of reflection peak at half height, is typically less than 100 nm due to limited birefringence of the material.[10]

Inspired by the nature, scientists have been able to conceptualize versatile photonic architectures, to provide appealing aesthetics and distinctive optical functions.[2,14–16] Tremendous efforts have been paid to engineer CLC materials, or more specifically, to control the helical organization of liquid crystal (LC) directors on the molecular scale. For instance, light-addressable or thermal-responsive chiral dopants allow tuning of the reflection wavelength.[17–20] Manipulation of the helical pitch direction or distribution provides an accessible route to realize beam steering, light diffraction, scattering or broadband reflection.[7,21–26] Coupling helical structures of the opposite handedness can achieve hyper-reflectivity, defined as the ability to reflect both left- and right-handed circularly polarized light (L-CPL and R-CPL).[27–32] In crosslinked CLC polymers, the distortion of helical structure generates polarization-dependent pseudo-Bragg reflectors and hyper-reflectivity.[33–35]

In terms of helix engineering, a variety of strategies and tools have been developed to produce the different delicate structures.[36–38] Among all options, photopolymerization-enforced stratification (PES) holds an important position, as the combination of polymer and CLC materials is versatile in LC-based functional devices.[38,39] PES refers to the formation of layered structures upon the application of photopolymerization in LC/polymer materials. In general, a spatially variant light

intensity, or energy absorption of the incident light, or a field induced spatial pattern is required to realize PES. In the context of CLCs, PES has been previously employed to produce flexible temperature-responsive reflectors.[19,20] However, a UV absorber is required to realize the vertical light intensity gradient and subsequent stratification. In addition, a non-mesogenic monomer is usually used to form the stratified polymer top layer, which serves as a protecting layer.

In this work, we describe a novel strategy to realize PES via a sequential polymerization and autonomous phase separation mechanism. Enabled by such strategy, hyper-reflectivity, instead of typical cholesteric reflection, successfully emerge from a single-layered chiral CLC system. Specifically, we use two chiral dopants of opposite handedness, with one being polymerizable and the other not. The mixture remains cholesteric with reflection towards CPL of a single handedness, as determined by the majority-rules principle.[40] PES is the key to break down the individual chiral contributions of the opposite chiral additives.[38] Upon photopolymerization, the system undergoes a three-stage phase separation process to form the stratified structure at the end, with two chiral dopants spontaneously phase separating into different layers, resulting into reflections towards CPL of the opposite handedness. This emergent approach to engineer hyper-reflective CLCs not only offers a new route to realize PES, but also enables excellent optical performance, stimuli-responsiveness, as well as the flexibility to adjust the center wavelength of hyper-reflection.

2 EXPERIMENTAL SECTION

Materials: The right-handed chiral diacrylate **1** (LC 756), diacrylate **2** (RM 257), monoacrylate **3** (RM 105) and left-handed chiral dopant **4** (S1011) was purchased from Jiangsu Hecheng Display Technology Co., Ltd. (Nanjing, China). The small-molecule LC **6** (4-Cyano-4'-pentylbiphenyl, 5CB) was obtained from Jiangsu Creative Electronic Chemicals (Nanjing, China). The photoinitiator **5** (Irgacure 651) was received from

Tianjin Heowns Biochem LLC. Homogeneous alignment was provided by an alignment layer of poly(vinyl alcohol) (PVA) obtained from Sigma-Aldrich. The compositions of hyper-reflective samples are summarized in Table 2.

Sample Preparation: To obtain LC cells with homogeneous alignment with anti-parallel rubbing at the top and bottom substrate, 2×2 cm^2 indium tin oxide (ITO) coated glasses were cleaned by ultrasonication in acetone and then ethanol for 30 minutes, respectively, followed by treatment of UV-ozone (BZS250GF-TC, Shenzhen HWOTECH Co., Ltd., Shenzhen, China) for 20 minutes. The PVA layer was spin-coated onto the ITO glass by using 5 wt.% PVA-water solution at 2000 rpm for 30 seconds. After drying, the PVA layer was rubbed with velvet cloth along one direction. Two pieces of ITO glasses were connected using UV glue containing 40 μm spacers to form the cell. The LC mixtures were prepared by weighing the components in the desired ratios and subsequently dissolving in dichloromethane (DCM) to ensure good mixing. The mixtures were kept at 50 °C for 6 hours to evaporate the solvent completely. Afterwards, the LC mixtures were filled into the cell at 50 °C and cooled down to room temperature. The cells were then exposed to UV light of 1.5 $mW \cdot cm^{-2}$ in intensity for 1 hour.

Characterization: The transmission spectra were measured using spectrophotometer Ocean Optics Maya 2000pro (Ocean Optics, Dunedin, USA) with ITO glass used as the baseline. Circularly polarized light (CPL) was obtained with a linear polarizer in combination with a quarter-wave plate. Polarized optical microscopy (POM) images were measured on a Leica DM2700P (Wetzlar, Germany), equipped with a CCD camera (Leica Infinity 1-3C) of 24-bit resolution. In order to examine the cross-sectional morphology, a piece of LC cell was first immersed in liquid nitrogen for 1 minute, and then cracked from the center into two halves. The characterization was conducted using both POM in reflection mode with one piece of polarizer and scanning electron

microscopy (SEM, ZEISS Ultra 55, Heidenheim, Germany). Differential scanning calorimetry (DSC) were performed using a DSC1 from METTLER TOLEDO (Zurich, Switzerland).

3 RESULTS AND DISCUSSION

3.1 Emergent Hyper-reflectivity in Cholesteric Liquid Crystals

The process of PES and emerging hyper-reflectivity from a chiral CLC system is illustrated in **Figure 1a**. We prepare a mixture consisting of reactive mesogens (RMs), non-polymerizable LCs, and a photoinitiator to realize PES (Figure 1b and **Table 2**, red). The design is inspired by previous work,[41] in which a homogeneous mixture containing non-mesogenic monomers and non-polymerizable LCs was used to fabricate a stratified coating on flexible polyethylene terephthalate (PET) substrates *via* photopolymerization. We use two chiral dopants **1** and **4** of the opposite handedness, with **1** being polymerizable and **4** non-polymerizable. We begin by examining three formulations with different chiral dopant concentrations. In this series, the concentration of **1** is fixed at 4.7 wt.%, while the concentration of **4** increases monotonically from 1.5 to 2.1 wt.%. Diacrylate **2**, monoacrylate **3**, and photoinitiator **5** are fixed at the concentrations of 11.0, 30.0, and 0.1 wt.%, with the rest being the small-molecule LC **6**. The mixtures are filled into planar aligned LC cells with a thickness of 40 μm. Before photopolymerization, all three cells exhibit around 50% reflection towards unpolarized light (**Figure S1**, top row). The reflection arises from the presence of a cholesteric phase, as confirmed by polarized optical microscopy (POM) observations (Figure 1c). Further analysis shows the reflection towards left-handed circularly polarized light (L-CPL) is close to zero, while that of right-handed circularly polarized light (R-CPL) is almost 100%. The results indicate that the right-handed chiral dopant **1** dominates in these mixtures, and the majority-rules principle takes effect. The helical twisting power (HTP) values for chiral dopants **1** and **4** also support

above results (**Table S1**). The estimation of cholesteric pitches based on the HTP values agrees well with the center wavelengths of the observed reflection peaks. As the concentration of **4** increases, the reflection peak redshifts.

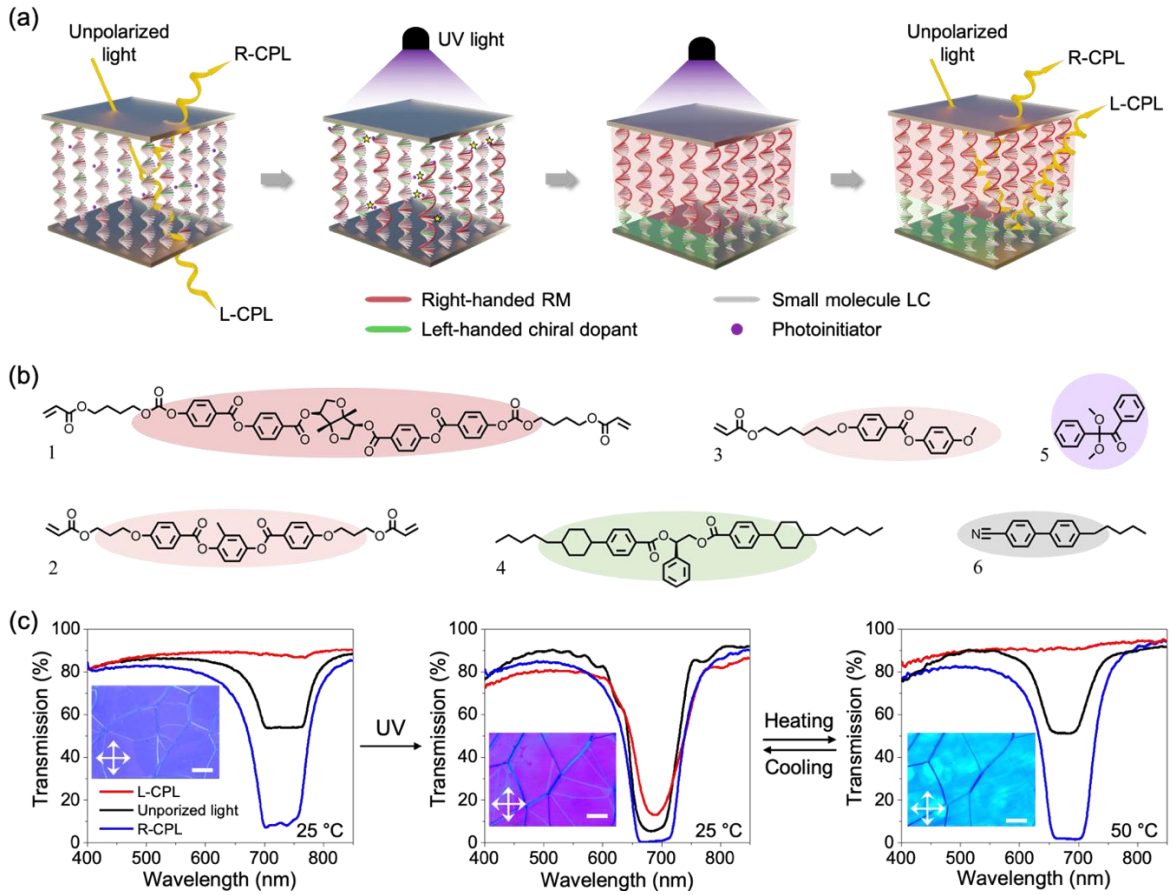

Figure 1. Principle of the formation of hyper-reflectivity. (a) Schematic of the photopolymerization-enforced stratification process to produce hyper-reflectivity. (b) Chemical structures of the materials used in the starting mixture. (c) (From left to right) Transmission spectra of the hyper-reflective sample before and after photopolymerization at 25 °C, which exhibits reversible changes when switched between 25 and 50 °C. The inserts are polarized optical microscopy (POM) images of the corresponding states (transmission mode). The scale bars are 50 μm.

We then conduct photopolymerization using a 365 nm LED lamp with a relatively weak intensity of 1.5 mW·cm^{-2} for 1 hour. After photopolymerization, the LC cells reflect L-CPL, while the reflection towards R-CPL remains and blue shifts slightly

(Figure S1, bottom row). The L-CPL reflection peaks appear towards lower wavelengths as the concentration of **4** is increased. At a concentration of 1.8 wt.%, the L-CPL and R-CPL reflection peaks overlap and produce an overall reflection over 90% towards unpolarized light, *i.e.*, hyper-reflectivity (Figure 1c). The characteristic oily streak texture for CLCs can still be observed under POM (Figure 1c), suggesting that the original cholesteric structure is preserved upon photopolymerization.[42] The hyper-reflective peak demonstrates a reversible change to typical CLC reflection as temperature increases, which will be discussed in detail later. A brief comparison to previously reported hyper-reflective CLCs strategies is shown in **Table 1**, where our method stands out as a facile and effective approach.

Table 1 Comparison of various methods for the creation of hyper-reflective CLC devices.

Methods	Lowest / baseline transmittance (unpolarized)[1]	Availability of materials[2]	Ease of processing	Responsiveness
Thermally induced helicity inversion[27]	28% / ~100%	Poor	Moderate	No
Light induced helicity inversion[30]	25% / 85%	Poor	Moderate	No
Wash-out/refill[28,29]	0% / 80%	Good	Difficult	Yes
Multi-layer stacking[31,32]	13% / 83%	Good	Difficult	No
3D helical structure engineering[33]	20% / 90%	Poor	Moderate	No
Distorted cholesteric structure[34,35]	0% / 80%	Good	Moderate	Yes
This work	5% / 90%	Good	Easy	Yes

[1] The lowest transmittance is taken from the hyper-reflective band. The baseline transmittance reflects the internal optical loss of the device.
[2] This term is judged by whether special chemicals that are not commercially available are used or not.

3.2 Mechanism of the Emergent Hyper-reflectivity

The appearance of L-CPL reflection and hyper-reflectivity confirm the phase separation between two chiral dopants of opposite handedness. Since there is no strong

UV absorber other than photoinitiator **5** existing in the starting mixture, there is no apparent gradient for light intensity inside the LC cell (**Figure S2**). The mechanism as described in previous reports,[19,20,39] cannot be applied to this stratification case. We therefore conduct *in-situ* monitoring of reflection band during the photopolymerization process to understand the mechanism (**Figure 2a** and **Figure S3**). Both the reflection towards R-CPL and L-CPL are tracked, which together will give the result for unpolarized light. Changes of the reflectance and center wavelength over the period of photopolymerization are plotted in Figure 2b. It is noted that for easy understanding, the reflectance value is calculated by subtracting the transmittance value directly. According to the results, the whole PES process can be roughly divided into three stages, as marked by different colors in the plot.

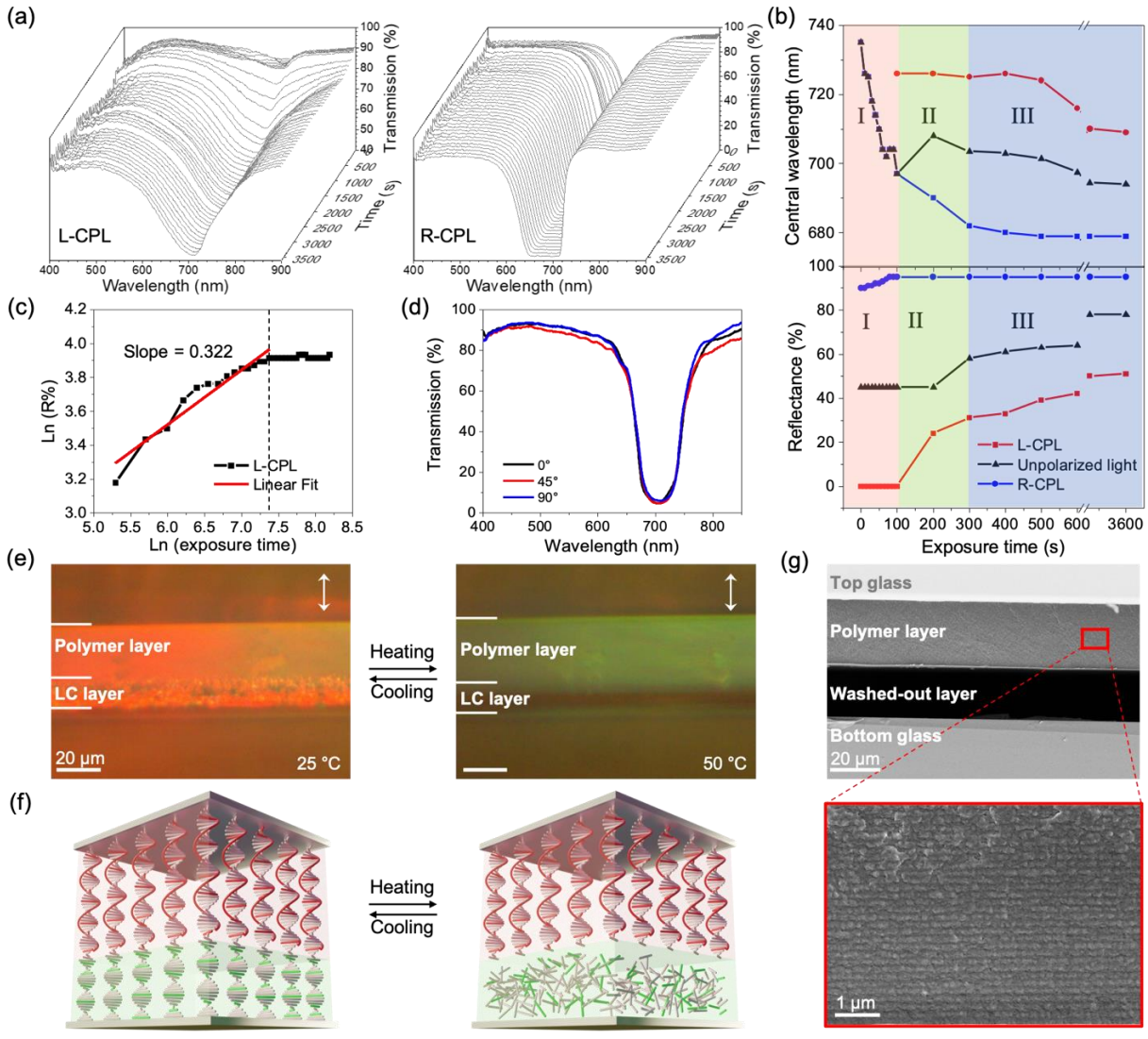

Figure 2. Mechanism for the formation of hyper-reflective CLC. (a) *In-situ* tracking of transmittance of L-CPL and R-CPL during photopolymerization. (b) The changes in reflection peak of L-CPL, R-CPL, and unpolarized light as a function of UV exposure time. (c) The reflectance of L-CPL is shown as a function of exposure time on a log-log plot, which gives a slope of ~0.322 for the early stage of growth. (d) Transmission spectra of the hyper-reflective sample measured using linearly polarized light at different incident angles with respect to the rubbing direction of the alignment layer. (e) POM images show the cross-section of hyper-reflective sample at 25 and 50 °C. The pictures are snapshots from Movie S1. (f) Schematic of the structure changes upon heating and cooling. (g) Scanning electron microscopy image shows the cross-section of hyper-reflective device after solvent extraction of small-molecule LC followed by drying (top). The magnified view of top polymer layer is shown on the bottom.

Stage I lasts about 100 seconds, during which the whole LC cell is photopolymerized when the UV light penetrates the sample with little attenuation. In this stage, the R-CPL as well as the unpolarized light reflection peak gradually blue shifts, due to the polymerization effect that will cause the cholesteric pitch to slightly decrease as a result of volume shrinkage.[43] There is no L-CPL reflection, as before the photopolymerization.

Stage II spans approximately from 100 to 300 seconds. The polymerization continues, and the R-CPL reflection further blue-shifts. Meanwhile, a L-CPL reflection appears near the R-CPL reflection, which remains almost in the same position but grows in intensity. This is presumably because the polymerized sample begins to phase separate into a polymer phase and a unpolymerized LC mixture phase, due to unfavorable thermodynamic interactions between the highly crosslinked polymer and unpolymerized LC mixture.[44] Since only chiral dopant **4** is secreted into the unpolymerized LC mixture phase, a left-handed cholesteric structure that reflects L-

CPL forms. Following the lever rule[45], this phase has a constant composition, which explains the nearly unchanged center wavelength of the growing L-CPL reflections.

After 300 seconds, the system proceeds to the Stage III, in which the R-CPL reflection does not change while L-CPL reflection grows further in intensity. During this time period, the phase separation continues and the thickness of the unpolymerized LC mixture phase increases. As a result, the L-CPL reflection grows in intensity, following a power-law behavior with the order being close to 1/3 in the early stage (Figure 2c). This result is consistent with previously reported kinetics for a phase separated system.[46,47] As for the R-CPL reflection, the reason that the center wavelength remains nearly the same is presumably due to the following reasons: First, the volume shrinkage due to photopolymerization is largely complete at this point. Second, phase separation drives not only the unpolymerized LC mixture phase, but also the polymer phase into a thermodynamically stable state, whose composition is also constant. The polymerization of mesogenic host (molecule **2** and **3**) and the leaving of small molecular LC **6** result in a different LC host environment. The polymerization of chiral dopant **1** will decrease its HTP value,[24,48] while the leaving of nonpolymerizable chiral dopant **4** effectively increases the right-handed twisting effect. All these phenomena together determine the center wavelength the R-CPL reflection (**Figure S4**). Thanks to the carefully adjusted composition, we can obtain overlapped L-CPL/R-CPL reflections and thus hyper-reflectivity after the phase separation (Figure S1). In addition, the relatively weak UV intensity is crucial for our design, which allows the phase separation to happen and the unreacted components to fully diffuse into the final bi-layer structure (**Figure S5**).

To further verify the proposed mechanism, we conduct a heating experiment on the hyper-reflective sample. The LC cell is heated to 50 °C, well above the clearing point (32.8 °C) of molecule **6** (**Figure S6**). The transmission spectrum of the sample shows a distinct change where the hyper-reflectivity disappears (Figure 1c). The reflection towards L-CPL vanishes completely, leaving the reflection towards R-CPL nearly

unchanged. The total reflection of unpolarized light decreases to around 50%, similar to a device based on a single layer of CLCs. Additional measurements show that the transmission/reflection is independent of the polarization direction of incoming linearly polarized light (LPL) (Figure 2d).[17] This allows us to study the changes upon heating by investigating a cross-section obtained by intersecting the cell in the middle, and *in-situ* monitoring the evolution of the cross-sectional morphology using POM (**Movie S1**). At room temperature of 25 °C, a bilayer structure can be clearly observed due to different colors (Figure 2e). Upon heating, the color of top layer transits from light orange to green, while the bottom layer turns dark from a grainy orange color. The changes are fully reversible. Both the cross-sectional morphology and the transmission spectrum recover after cooling back to 25 °C. These results agree well with our proposed mechanism. The polymer phase is attached to the top substrate and form a uniform layer, presumably due to the incidence of UV light from this side.[49,50] The color change of top polymer layer indicates the existence of small-molecule LC **6**, which we will further discuss below. The phase-separated unpolymerized LC mixture forms the bottom LC layer, which becomes isotropic after being heated to 50 °C and loses the cholesteric structure (Figure 2f). As a result, its appearance becomes dark between crossed polarizers, and its reflection peak vanishes.

We conduct additional experiments to characterize the top polymer layer. A good solvent for 5CB, cyclohexane, is used to soak the cracked LC cell and wash out the small molecule LCs. After drying, scanning electron microscopy (SEM) is utilized to examine the cross-section. The remaining polymer layer is attached to the top glass substrate after the process (Figure 2g). The hyper-reflectivity of the device also disappears after solvent treatment. The dried sample only reflects R-CPL, at a lower wavelength compared to the original device (**Figure S7**). Periodic layered structures can be found in the zoomed-in view of the polymer layer, which again confirms its cholesteric nature and supports our proposed mechanism. The measured layer periodicity (280.8 nm) is largely uniform over the entire thickness, and agrees well with

the center wavelength of reflection peak (~450 nm).

Based on the spectral and morphological analysis, we can quantitatively estimate the composition of the bilayer (**Figure S8** and **Table S2**). The HTP values of two chiral dopants are calculated in different mixtures by reflection peak and average refractive index. Assuming complete consumption of all the RMs to form the top polymer layer, and the same density for the polymer and LC layer, we can analyze all three samples shown in Figure S1. It turns out the concentration of chiral dopant **4** has little influence on the phase separation process. About 44% of molecule **6** and 84% of molecule **4** in the starting mixture are squeezed to the bottom LC layer after photopolymerization for all three samples. The stratification process is not influenced by the enantiomeric form of chiral dopant **4** either (**Table S2** and **Figure S9**). These results indicate no preferential interaction depending on the handedness, *i.e.*, chiral interaction, exists between two chiral dopants **1** and **4**, presumably because the structures of their chiral centers are quite different. The phase separation process is primarily determined by the enthalpic interactions among different components. Consequently, our strategy to realize PES and fabricate hyper-reflective devices is universal. We could replace molecule **1** and **4** with other chiral dopants and maintain hyper-reflectivity (**Figure S10**).

3.3 Modulation and Application of the Hyper-reflective Devices

By modulating the concentration of chiral dopants **1** and **4**, we can adjust the position of the hyper-reflective peak. The center wavelength can be shifted from 719 to 472 nm (**Figure 3a** and 3b), and even further into the ultraviolet or oppositely to the infrared regime. More interestingly, we notice that the ratios between the mass concentrations of these two chiral dopants remain nearly the same for four samples presenting red, yellow, green and blue colors (**Table 2**). Cross-sectional SEM observations indicate similar bilayer structures to Figure 2f (**Figure S11**). The pitch in the collapsed polymer layer decreases monotonically as the concentration of chiral

dopants increases. The results are understandable since the mechanism that dictates the formation of hype-reflectivity remains unchanged. Moreover, the results provide a facile strategy to design and fabricate hyper-reflective devices. When two chiral dopants of opposite handedness are chosen, a mass ratio can be determined for a given achiral LC system following the experiments shown in Figure S1. If mixed using such characteristic ratio, the two chiral dopants can act together like a new chiral dopant bundle. By varying the concentration of this chiral dopant bundle, hyper-reflectivity can be obtained at a broad range of wavelengths. This chiral dopant bundle behaves like it has a characteristic HTP value, but it shows hyper-reflections rather than normal cholesteric reflection.

In addition, we can utilize a photomask to design and fabricate patterned hyper-reflective devices (Figure 3c). In the demo the heart shape is exposed to UV light to initiate photopolymerization and stratification. As a result, it shows hyper-reflection at room temperature, while the background only reflects R-CPL due to its cholesteric structure. The hyper-reflection disappears when the device is heated to 50 °C, and fully recovers when cooled down.

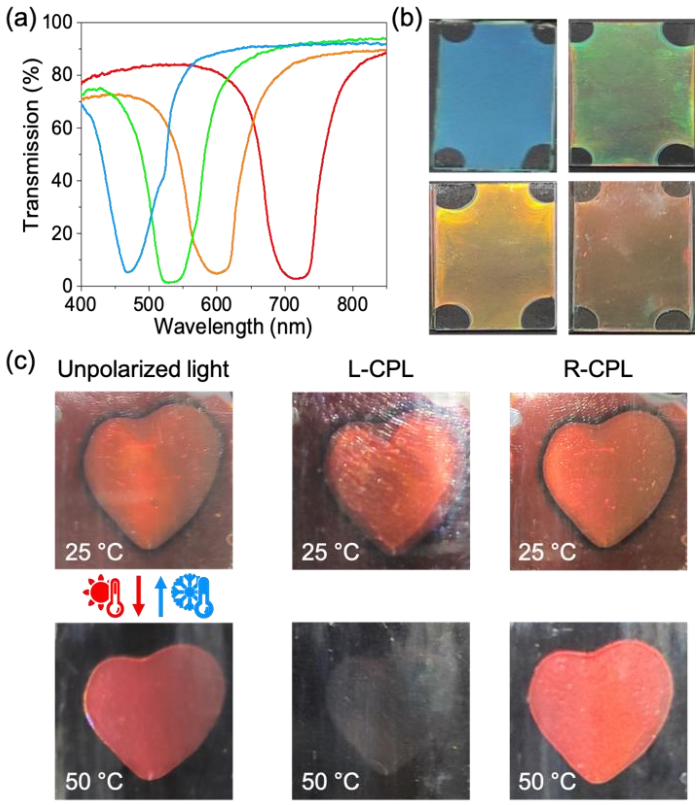

Figure 3. Hyper-reflective CLC devices with various color and pattern design. (a) Transmission spectra of unpolarized light for the red, yellow, green, and blue colored hyper-reflective samples. (b) Snapshots of the colored samples on a black background. (c) Patterned hyper-reflective device with a heart shape viewed under unpolarized light, R-CPL and L-CPL at different temperatures. The width of sample is 2 cm.

Table 2 Mixture compositions (wt. %) used to prepare the hyper-reflective red, yellow, green and blue samples.

Sample	**Achiral LC mixture**		**Chiral dopant 1**	**Chiral dopant 4**	**Mass ratio** (dopant **1** / dopant **4**)
	Molecule **2**/**3**/**5**	Molecule **6**			
Red	11.0 / 30.0 / 0.1	52.4	4.9	1.8	2.7
Yellow		51.4	5.4	2.1	2.6
Green		50.6	5.9	2.4	2.5
Blue		49.8	6.4	2.7	2.4

With the knowledge on the fabrication of hyper-reflective devices from our chosen material system, we then proceeded to explore the responsiveness of such devices, in particular the electrical and thermal response (**Figure 4**). When an electric field is applied to the bilayer hyper-reflective sample, the small molecule LC layer is likely to undergo changes from the initial planar aligned state to the focal conic state, and then to the cholesteric fingerprint state, while the polymer layer is less likely to be influenced thanks to the crosslinked structure (**Figure S12**).[7,51] As a result, the sample first becomes pale and hazy, then nearly transparent under L-CPL, due to the changes happening in the LC layer. In contrast, the changes under R-CPL and unpolarized light are much less obvious. When heated from 25 to 50 °C, the color of sample is still red under unpolarized light and R-CPL, but is no longer visible with L-CPL. The reflection of L-CPL vanishes as the small molecule LC layer becomes isotropic. These results indicate the possibility to control hyper-reflectivity and other optical properties of the device.

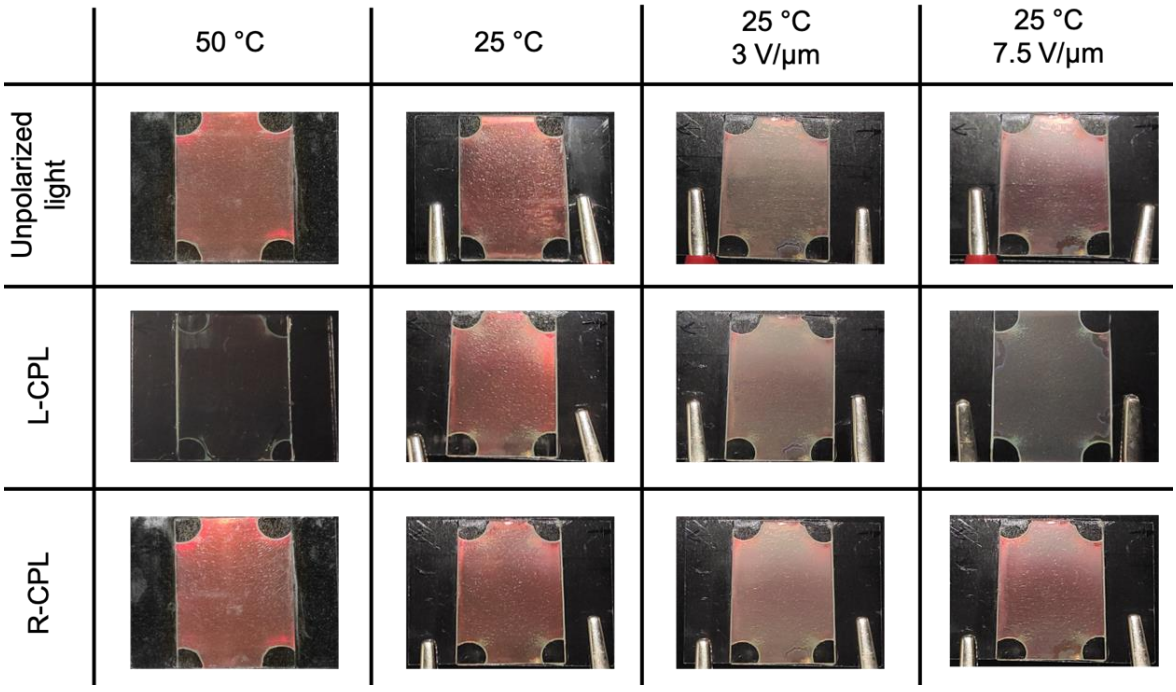

Figure 4. Photographs of a hyper-reflective device viewed under unpolarized light, R-CPL and L-CPL at different temperatures and electric field strengths. The width of

sample is 2 cm.

4 CONCLUSIONS

In conclusion, we developed a novel photopolymerization-enforced stratification-based strategy to achieve hyper-reflective CLCs. Rather than presenting the photopolymerization-induced diffusion, the observed PES follows a sequential polymerization and phase separation mechanism. Thermodynamic interactions among all components dictate the phase separation and stratification process. The power of this PES strategy is well demonstrated through the emergence of hyper-reflectivity in a single-layered CLC, which is formed by a chiral dopant bundle together with an achiral LC mixture. The bundle consists of two chiral dopants of opposite handedness, one being polymerizable and the other not. When paired at a characteristic ratio, as determined by the nature of two components, the chiral dopant bundle can be used as a normal chiral dopant for nematic LCs. By adjusting the concentration of chiral dopant bundle in the achiral LC mixture, hyper-reflectivity can be facilitated at a broad range of wavelengths. This novel PES strategy not only enables facile helix engineering in CLCs to produce hyper-reflectivity, but also offers great flexibility to introduce additional stimuli responsiveness to the hyper-reflective CLC devices, which holds great promises in many areas, such as digital displays, lasing, optical storage, and smart windows.

Supporting Information

The Supporting information is available free of charge online.

- Measurement of HTP values, formulations with different chiral dopant concentrations, absorption of the sample before photopolymerization, experimental setup used for *in-situ* monitoring, influence of stratification on the R-CPL reflection, influence of UV intensity for photopolymerization, DSC characterization, transmission spectrum of the hyper-reflective sample after removing small-molecule LCs, estimation of the composition of bilayer structure, comparison between enantiomers S1011 and R1011, hyper-reflective devices based on different chiral dopants, measurement of cholesteric pitches in the polymer layer, and electrical response of the hyper-reflective CLC device. (PDF)
- POM *in-situ* monitoring the evolution of the cross-sectional morphology during heating of the hyper-reflective CLC. (video)

Author contributions

Wei Zhao (WZ) and Laurens T. de Haan (LTH) conceived the research. WZ, LTH, and Qunmei Wei (QMW) designed the material mixture and preparation conditions. QMW, Pengrong Lv, Yang Zhang and Jiwen Zhang performed the experiments and characterizations. QMW, Zhuofan Qin, Ding Wang and Ben Bin Xu (BBX) conducted the analysis and presentation of experimental data. WZ, LTH, BBX and Dirk J. Broer discussed and proposed the mechanism of stratification. QMW wrote the original version of the manuscript. LTH, BBX, Liming Ding and WZ revised the manuscript. WZ, Jiawen Chen and Guofu Zhou provided important resource for this research investigation.

Notes

The authors declare that they have no conflict of interest.

Acknowledgements

The authors want to thank Dr. Albert P.H.J. Schenning, Dr. Danqing Liu for useful discussions. This work was supported financially by National Key R&D Program of China (No. 2020YFE0100200), Science and Technology Program of Guangzhou (No. 2019050001), Special Projects in Key Areas of Guangdong Provincial Department of Education (No. 2020ZDZX2064), Program for Chang Jiang Scholars and Innovative Research Teams in Universities (No. IRT_17R40), Guangdong Provincial Key Laboratory of Optical Information Materials and Technology (No. 2017B030301007), Industry-University-Research Cooperation Project of Zhuhai City (No. ZH22017001200043PWC), MOE International Laboratory for Optical Information Technologies, the 111 Project and Yunnan expert workstation (No. 202005AF150028).

References

(1) Droguet, B. E.; Liang, H.-L.; Frka-Petesic, B.; Parker, R. M.; De Volder, M. F. L.; Baumberg, J. J.; Vignolini, S. Large-Scale Fabrication of Structurally Coloured Cellulose Nanocrystal Films and Effect Pigments. *Nat. Mater.* **2022**, *21*, 352–358. https://doi.org/10.1038/s41563-021-01135-8.

(2) Wang, L.; Urbas, A. M.; Li, Q. Nature-Inspired Emerging Chiral Liquid Crystal Nanostructures: From Molecular Self-Assembly to DNA Mesophase and Nanocolloids. *Adv. Mater.* **2020**, *32* (41), 1801335. https://doi.org/10.1002/adma.201801335.

(3) Tortora, M. M. C.; Mishra, G.; Prešern, D.; Doye, J. P. K. Chiral Shape Fluctuations and the Origin of Chirality in Cholesteric Phases of DNA Origamis. *Sci. Adv.* **2020**, *6* (31), eaaw8331. https://doi.org/10.1126/sciadv.aaw8331.

(4) Zhao, J.; Gulan, U.; Horie, T.; Ohmura, N.; Han, J.; Yang, C.; Kong, J.; Wang, S.; Xu, B. B. Advances in Biological Liquid Crystals. *Small* **2019**, *15* (18), 1900019. https://doi.org/10.1002/smll.201900019.

(5) Mitov, M. Cholesteric Liquid Crystals in Living Matter. *Soft Matter* **2017**, *13* (23), 4176–4209. https://doi.org/10.1039/C7SM00384F.

(6) Qin, L.; Gu, W.; Wei, J.; Yu, Y. Piecewise Phototuning of Self-Organized Helical Superstructures. *Adv. Mater.* **2018**, *30* (8), 1704941. https://doi.org/10.1002/adma.201704941.

(7) Bisoyi, H. K.; Bunning, T. J.; Li, Q. Stimuli-Driven Control of the Helical Axis of Self-Organized Soft Helical Superstructures. *Adv. Mater.* **2018**, *30* (25), 1706512. https://doi.org/10.1002/adma.201706512.

(8) Bisoyi, H. K.; Li, Q. Light-Directed Dynamic Chirality Inversion in Functional Self-Organized Helical Superstructures. *Angew. Chem. Int. Ed.* **2016**, *55* (9), 2994–3010. https://doi.org/10.1002/anie.201505520.

(9) Wang, C.; Wang, D.; Kozhevnikov, V.; Dai, X.; Turnbull, G.; Chen, X.; Kong, J.; Tang, B. Z.; Li, Y.; Xu, B. B. A Flexible Topo-Optical Sensing Technology with Ultra-High Contrast. *Nat. Commun.* **2020**, *11* (1), 1448. https://doi.org/10.1038/s41467-020-15288-8.

(10) Mitov, M. Cholesteric Liquid Crystals with a Broad Light Reflection Band. *Adv. Mater.* **2012**, *24* (47), 6260–6276. https://doi.org/10.1002/adma.201202913.

(11) Ryabchun, A.; Sakhno, O.; Stumpe, J.; Bobrovsky, A. Full-Polymer Cholesteric Composites for Transmission and Reflection Holographic Gratings. *Adv. Opt. Mater.* **2017**, *5* (17), 1700314. https://doi.org/10.1002/adom.201700314.

(12) Hussain, S.; Park, S. Photonic Cholesteric Liquid-Crystal Elastomers with Reprogrammable Helical Pitch and Handedness. *ACS Appl. Mater. Interfaces* **2021**, *13* (49), 59275–59287. https://doi.org/10.1021/acsami.1c18697.

(13) Zhang, L.; Nie, Q.; Jiang, X.-F.; Zhao, W.; Hu, X.; Shui, L.; Zhou, G. Enhanced Bandwidth Broadening of Infrared Reflector Based on Polymer Stabilized Cholesteric Liquid Crystals with Poly(N-Vinylcarbazole) Used as Alignment Layer. *Polymers*

2021, *13* (14), 2238. https://doi.org/10.3390/polym13142238.
(14) Tadepalli, S.; Slocik, J. M.; Gupta, M. K.; Naik, R. R.; Singamaneni, S. Bio-Optics and Bio-Inspired Optical Materials. *Chem. Rev.* **2017**, *117* (20), 12705–12763. https://doi.org/10.1021/acs.chemrev.7b00153.
(15) Ryabchun, A.; Bobrovsky, A. Cholesteric Liquid Crystal Materials for Tunable Diffractive Optics. *Adv. Opt. Mater.* **2018**, *6* (15), 1800335. https://doi.org/10.1002/adom.201800335.
(16) Qing, X.; Liu, Y.; Wei, J.; Zheng, R.; Zhu, C.; Yu, Y. Phototunable Morpho Butterfly Microstructures Modified by Liquid Crystal Polymers. *Adv. Opt. Mater.* **2019**, *7* (3), 1801494. https://doi.org/10.1002/adom.201801494.
(17) Wang, H.; Bisoyi, H. K.; Wang, L.; Urbas, A. M.; Bunning, T. J.; Li, Q. Photochemically and Thermally Driven Full-Color Reflection in a Self-Organized Helical Superstructure Enabled by a Halogen-Bonded Chiral Molecular Switch. *Angew. Chem. Int. Ed.* **2018**, *57* (6), 1627–1631. https://doi.org/10.1002/anie.201712781.
(18) Qin, L.; Gu, W.; Wei, J.; Yu, Y. Piecewise Phototuning of Self-Organized Helical Superstructures. *Adv. Mater.* **2018**, *30* (8), 1704941. https://doi.org/10.1002/adma.201704941.
(19) Khandelwal, H.; Heeswijk, E. P. A. van; Schenning, A. P. H. J.; Debije, M. G. Paintable Temperature-Responsive Cholesteric Liquid Crystal Reflectors Encapsulated on a Single Flexible Polymer Substrate. *J. Mater. Chem. C* **2019**, *7* (24), 7395–7398. https://doi.org/10.1039/C9TC02011J.
(20) Ranjkesh, A.; Yoon, T.-H. Fabrication of a Single-Substrate Flexible Thermoresponsive Cholesteric Liquid-Crystal Film with Wavelength Tunability. *ACS Appl. Mater. Interfaces* **2019**, *11* (29), 26314–26322. https://doi.org/10.1021/acsami.9b05112.
(21) Zheng, Z.; Li, Y.; Bisoyi, H. K.; Wang, L.; Bunning, T. J.; Li, Q. Three-Dimensional Control of the Helical Axis of a Chiral Nematic Liquid Crystal by Light. *Nature* **2016**, *531* (7594), 352–356. https://doi.org/10.1038/nature17141.
(22) Kobashi, J.; Yoshida, H.; Ozaki, M. Planar Optics with Patterned Chiral Liquid Crystals. *Nature Photon.* **2016**, *10* (6), 389–392. https://doi.org/10.1038/nphoton.2016.66.
(23) Sun, J.; Lan, R.; Gao, Y.; Wang, M.; Zhang, W.; Wang, L.; Zhang, L.; Yang, Z.; Yang, H. Stimuli-Directed Dynamic Reconfiguration in Self-Organized Helical Superstructures Enabled by Chemical Kinetics of Chiral Molecular Motors. *Adv. Sci.* **2018**, *5* (2), 1700613. https://doi.org/10.1002/advs.201700613.
(24) Wang, X.; He, J.; Wei, Q.; Zhang, Y.; Li, Y.; Zhang, Z.; Zhao, W.; Zhou, G. Influence of Molecular Weight on Helical Twisting Power of Oligomer Chiral Dopants. *J. Mol. Liq.* **2021**, *339*, 116816. https://doi.org/10.1016/j.molliq.2021.116816.
(25) Hikmet, R. a. M.; Kemperman, H. Electrically Switchable Mirrors and Optical Components Made from Liquid-Crystal Gels. *Nature* **1998**, *392* (6675), 476–479.

https://doi.org/10.1038/33110.
(26) Hu, X.; Zeng, W.; Yang, W.; Xiao, L.; De Haan, L. T.; Zhao, W.; Li, N.; Shui, L.; Zhou, G. Effective Electrically Tunable Infrared Reflectors Based on Polymer Stabilised Cholesteric Liquid Crystals. *Liq. Cryst.* **2019**, *46* (2), 185–192. https://doi.org/10.1080/02678292.2018.1483038.
(27) Mitov, M.; Dessaud, N. Going beyond the Reflectance Limit of Cholesteric Liquid Crystals. *Nat. Mater.* **2006**, *5* (5), 361. https://doi.org/10.1038/nmat1619.
(28) Guo, J.; Chen, F.; Qu, Z.; Yang, H.; Wei, J. Electrothermal Switching Characteristics from a Hydrogen-Bonded Polymer Network Structure in Cholesteric Liquid Crystals with a Double-Handed Circularly Polarized Light Reflection Band. *J. Phys. Chem. B* **2011**, *115* (5), 861–868. https://doi.org/10.1021/jp109193m.
(29) McConney, M. E.; Tondiglia, V. P.; Hurtubise, J. M.; Natarajan, L. V.; White, T. J.; Bunning, T. J. Thermally Induced, Multicolored Hyper-Reflective Cholesteric Liquid Crystals. *Adv. Mater.* **2011**, *23* (12), 1453–1457. https://doi.org/10.1002/adma.201003552.
(30) Sun, J.; Yu, L.; Wang, L.; Li, C.; Yang, Z.; He, W.; Zhang, C.; Zhang, L.; Xiao, J.; Yuan, X.; Li, F.; Yang, H. Optical Intensity-Driven Reversible Photonic Bandgaps in Self-Organized Helical Superstructures with Handedness Inversion. *J. Mater. Chem. C* **2017**, *5* (15), 3678–3683. https://doi.org/10.1039/C7TC00534B.
(31) Khandelwal, H.; Loonen, R. C. G. M.; Hensen, J. L. M.; Schenning, A. P. H. J.; Debije, M. G. Application of Broadband Infrared Reflector Based on Cholesteric Liquid Crystal Polymer Bilayer Film to Windows and Its Impact on Reducing the Energy Consumption in Buildings. *J. Mater. Chem. A* **2014**, *2* (35), 14622–14627. https://doi.org/10.1039/C4TA03047H.
(32) Li, Y.; Liu, Y. J.; Dai, H. T.; Zhang, X. H.; Luo, D.; Sun, X. W. Flexible Cholesteric Films with Super-Reflectivity and High Stability Based on a Multi-Layer Helical Structure. *J. Mater. Chem. C* **2017**, *5* (41), 10828–10833. https://doi.org/10.1039/c7tc03915h.
(33) Kragt, A. J. J.; Hoekstra, D. C.; Stallinga, S.; Broer, D. J.; Schenning, A. P. H. J. 3D Helix Engineering in Chiral Photonic Materials. *Adv. Mater.* **2019**, *31* (33), 1903120. https://doi.org/10.1002/adma.201903120.
(34) Sol, J. A. H. P.; Sentjens, H.; Yang, L.; Grossiord, N.; Schenning, A. P. H. J.; Debije, M. G. Anisotropic Iridescence and Polarization Patterns in a Direct Ink Written Chiral Photonic Polymer. *Adv. Mater.* **2021**, *33* (39), 2103309. https://doi.org/10.1002/adma.202103309.
(35) Zhang, P.; Zhou, G.; de Haan, L. T.; Schenning, A. P. H. J. 4D Chiral Photonic Actuators with Switchable Hyper-Reflectivity. *Adv. Funct. Mater.* **2021**, *31* (9), 2007887. https://doi.org/10.1002/adfm.202007887.
(36) Ndaya, D.; Bosire, R.; Vaidya, S.; Kasi, R. M. Molecular Engineering of Stimuli-Responsive, Functional, Side-Chain Liquid Crystalline Copolymers: Synthesis, Properties and Applications. *Polym. Chem.* **2020**, *11* (37), 5937–5954. https://doi.org/10.1039/d0py00749h.

(37) del Pozo, M.; Sol, J. A. H. P.; Schenning, A. P. H. J.; Debije, M. G. 4D Printing of Liquid Crystals: What's Right for Me? *Adv. Mater.* **2022**, *34* (3), 2104390. https://doi.org/10.1002/adma.202104390.
(38) Zhao, W.; de Haan, L. T.; Broer, D. J.; Zhang, Y.; Lv, P.; Zhou, G. Photopolymerization-Enforced Stratification in Liquid Crystal Materials. *Prog. Polym. Sci.* **2021**, *114*, 101365. https://doi.org/10.1016/j.progpolymsci.2021.101365.
(39) Penterman, R.; Klink, S. I.; Koning, H. de; Nisato, G.; Broer, D. J. Single-Substrate Liquid-Crystal Displays by Photo-Enforced Stratification. *Nature* **2002**, *417* (6884), 55. https://doi.org/10.1038/417055a.
(40) Cao, H.; Zhu, X.; Liu, M. Self-Assembly of Racemic Alanine Derivatives: Unexpected Chiral Twist and Enhanced Capacity for the Discrimination of Chiral Species. *Angew. Chem. Int. Ed.* **2013**, *52* (15), 4122–4126. https://doi.org/10.1002/anie.201300444.
(41) Moirangthem, M.; Scheers, A. F.; Schenning, A. P. H. J. A Full Color Photonic Polymer, Rewritable with a Liquid Crystal Ink. *Chem. Commun.* **2018**, *54* (35), 4425–4428. https://doi.org/10.1039/C8CC02188K.
(42) The Nematic and Cholesteric Phases. In *Textures of Liquid Crystals*; John Wiley & Sons, Ltd, 2003; pp 51–74. https://doi.org/10.1002/3527602054.ch5.
(43) Broer, D. J.; Heynderickx, I. Three-Dimensionally Ordered Polymer Networks with a Helicoidal Structure. *Macromolecules* **1990**, *23* (9), 2474–2477. https://doi.org/10.1021/ma00211a012.
(44) Kamal, T.; Park, S. Shape-Responsive Actuator from a Single Layer of a Liquid-Crystal Polymer. *ACS Appl. Mater. Interfaces* **2014**, *6* (20), 18048–18054. https://doi.org/10.1021/am504910h.
(45) Smith, W. F.; Hashemi, J. *Foundations of Materials Science and Engineering*, 7th edition.; McGraw-Hill, 2022. pp. 373-377
(46) Gaulin, B. D. Kinetics of Spinodal Decomposition in One Dimension. *Phys. Rev. B* **1988**, *38* (10), 7184–7187. https://doi.org/10.1103/PhysRevB.38.7184.
(47) Singh, A.; Puri, S.; Dasgupta, C. Kinetics of Phase Separation in Polymer Mixtures: A Molecular Dynamics Study. *The Journal of Chemical Physics* **2014**, *140* (24), 244906. https://doi.org/10.1063/1.4884824.
(48) Heeswijk, E. P. A. van; Yang, L.; Grossiord, N.; Schenning, A. P. H. J. Tunable Photonic Materials via Monitoring Step-Growth Polymerization Kinetics by Structural Colors. *Adv. Funct. Mater.* **2020**, *30* (7), 1906833. https://doi.org/10.1002/adfm.201906833.
(49) Kang, S.-W.; Sprunt, S.; Chien, L.-C. Structure and Morphology of Polymer-Stabilized Cholesteric Diffraction Gratings. *Appl. Phys. Lett.* **2000**, *76* (24), 3516–3518. https://doi.org/10.1063/1.126692.
(50) Li, K.; Jiang, H.; Cheng, M.; Li, Y.; Yin, Z.; Luo, D.; Sun, X. W.; Liu, Y. J. Controlling Morphological and Electro-Optical Properties via the Phase Separation in Polymer/Liquid-Crystal Composite Materials. *Liq. Cryst.* **2020**, *47* (2), 238–247. https://doi.org/10.1080/02678292.2019.1641854.

(51) Mo, L.; Sun, H.; Liang, A.; Jiang, X.; Shui, L.; Zhou, G.; de Haan, L. T.; Hu, X. Multi-Stable Cholesteric Liquid Crystal Windows with Four Optical States. *Liq. Cryst.* **2021**, *49* (3), 289–296. https://doi.org/10.1080/02678292.2021.1962422.

TOC graphic

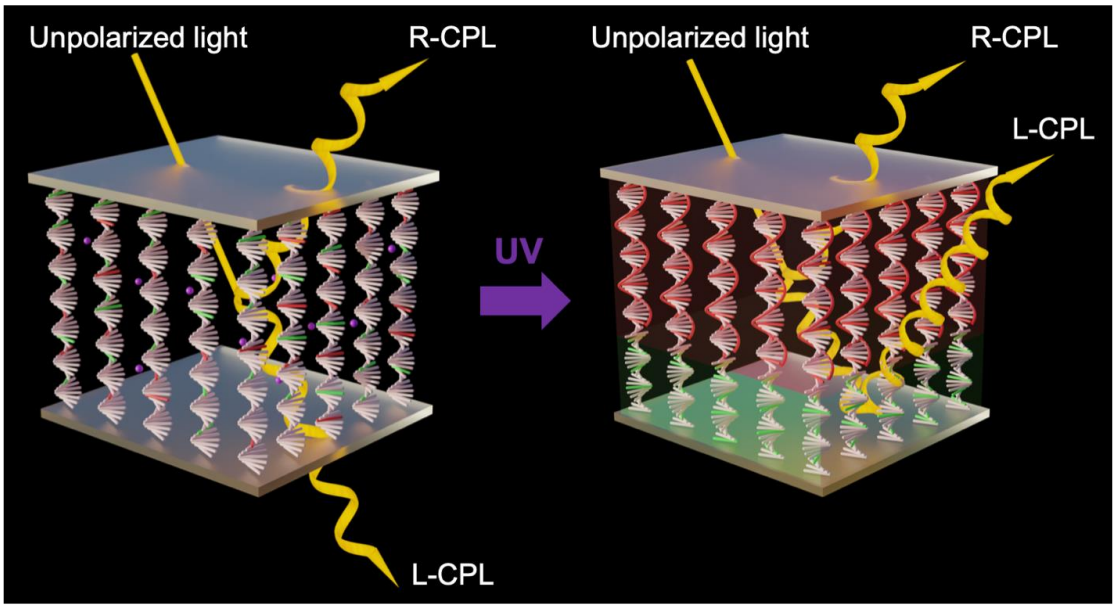
Unpolarized light
R-CPL
UV
L-CPL
Unpolarized light
R-CPL
L-CPL